that the Monte Carlo analysis does not employ the pessimistic approximations of (40) and (41).

IV. Conclusions

The concepts we have described and the results obtained are promising. Our approach is the most direct way of currently obtaining minimum cost designs under practical situations, at least in the worst case sense. It is felt that this work is a significant advance in the art of computer-aided design, since the approach permits the inclusion of all realistic degrees of freedom of a design and all physical phenomena that influence the subsequent performance.

The approach automatically creates a tradeoff between physical tolerances (implying the cost of the network), model parameter uncertainties (implying our knowledge of the network), the quality of the terminations, and, eventually, the cost of tuning. Our approach to mismatches permits input and output connecting lines of arbitrary length—an important step towards modular design.

The conventional computer-aided design process, which seeks a single nominal design or its extension which attempts to find a design center influenced by sensitivities (see, for example, Rauscher and Epprecht [9]), would normally be a preliminary investigation to find a starting point for the work we have in mind.

References

[1] J. W. Bandler, "Computer optimization of inhomogeneous waveguide transformers," *IEEE Trans. Microwave Theory Tech.*, vol. MTT-17, pp. 563–571, Aug. 1969.
[2] H. Tromp and G. Hoffman, "Computer optimization of 3 dB microstrip hybrids taking into account dispersive, coupling and junction effects," *Proc. 1973 European Microwave Conf.* (Brussels, Belgium, Sept. 1973), Paper A.12.4.
[3] J. W. Bandler, P. C. Liu, and J. H. K. Chen, "Worst case network tolerance optimization," *IEEE Trans. Microwave Theory Tech.*, vol. MTT-23, pp. 630–641, Aug. 1975.
[4] J. W. Bandler, P. C. Liu, and H. Tromp, "A nonlinear programming approach to optimal design centering, tolerancing and tuning," *IEEE Trans. Circuits and Systems*, vol. CAS-23, pp. 155–165, March 1976.
[5] H. J. Carlin and A. B. Giordano, *Network Theory*. Englewood Cliffs, N.J.: Prentice-Hall, 1964, pp. 331–334.
[6] H. M. Altschuler and A. A. Oliner, "Discontinuities in the center conductor of symmetric strip transmission line," *IRE Trans. Microwave Theory Tech.*, vol. MTT-8, pp. 328–339, May 1960.
[7] V. Nalbandian and W. Steenaart, "Discontinuities in symmetric striplines due to impedance steps and their compensations," *IEEE Trans. Microwave Theory Tech.*, vol. MTT-20, pp. 573–578, Sept. 1972.
[8] J. W. Bandler and J. H. K. Chen, "DISOPT—A general program for continuous and discrete nonlinear programming problems," *Int. J. Systems Science*, vol. 6, pp. 665–680, 1975.
[9] C. Rauscher and G. Epprecht, "Simplified approach to sensitivity optimization by use of scattering parameters," in *Proc. 1974 European Microwave Conf.* (Montreux, Switzerland, Sept. 1974), pp. 394–398.

Effect of the Magnetic Perturbation on Magnetostatic Surface-Wave Propagation

MAKOTO TSUTSUMI, MEMBER, IEEE, TUSHAR BHATTACHARYYA, AND NOBUAKI KUMAGAI, SENIOR MEMBER, IEEE

***Abstract*—This paper discusses the propagation of the magnetostatic surface wave in two ferrite slabs (namely, YIG and Ga-YIG) with different magnetic saturations, and considers a weak coupling in between them. The theoretical results are obtained by using the conventional perturbation technique which is subsequently supported by experiment. Further, the time delay in group velocity affected by the magnetic perturbation is treated theoretically.**

Manuscript received November 19, 1975; revised March 1, 1976. T. Bhattacharyya received financial assistance from Matsushita Research Institute, Tokyo, Japan, to carry out this research.

M. Tsutsumi and N. Kumagai are with the Department of Electrical Communication Engineering, Osaka University, Yamada Kami, Osaka 565, Japan.

T. Bhattacharyya is with the Department of Electrical Communication Engineering, Osaka University, Yamada Kami, Osaka 565, Japan, on leave from Jadavpur University, Calcutta 32, India.

I. Introduction

THE propagation loss associated with a magnetostatic surface wave on a YIG slab is relatively low [1]. Recently, a millimeter delay-line equalizer has been reported as one of the applications of these surface waves [2].

Since surface waves tend to concentrate the major part of their energy near the surface [3], this phenomenon can be utilized to couple the wave to other circuits through the surface to manipulate the propagation characteristic through this coupling. In particular, one problem that arises is the control of the propagation characteristic by changing the distance between the two interacting slabs. This type of problem has already been considered by

Ganguly *et al.* [4], [5] and Bongianni [6] who have suggested that a nondispersive delay line may be obtained with the help of two such interacting slabs. However, they treated the coupling between the two slabs when these have different anisotropic internal magnetic fields [5], [6]. The purpose of the present paper is to discuss the propagation of the magnetostatic surface wave in two ferrite slabs (namely, YIG and Ga-YIG) of different magnetic saturations with the existence of a weak coupling in between them. The theoretical results are obtained by using the conventional perturbation technique which is subsequently confirmed by experiment. The time delay of group velocity affected by the magnetic perturbation is also estimated theoretically.

II. Perturbed and Unperturbed Quantities

A. Perturbation Representation

In this section, the perturbation formula for such a magnetostatic case is developed. Let the unperturbed field quantities be designated as $\boldsymbol{E}_0$, $\boldsymbol{H}_0$, $\boldsymbol{D}_0$, and $\boldsymbol{B}_0$ and the corresponding perturbed quantities be $\boldsymbol{E}$, $\boldsymbol{H}$, $\boldsymbol{D}$, and $\boldsymbol{B}$. Thus the use of Maxwell's equations yields to

$$\nabla \times \boldsymbol{E} = -j\omega \boldsymbol{B} \qquad \nabla \times \boldsymbol{H} = j\omega \boldsymbol{D} \tag{1}$$

and

$$\nabla \times \boldsymbol{E}_0^* = j\omega \boldsymbol{B}_0^* \qquad \nabla \times \boldsymbol{H}_0^* = -j\omega \boldsymbol{D}_0^*. \tag{2}$$

In the previous expressions, the asterisk refers to the complex conjugate. As the medium, treated here, is a ferrite medium—the relation between the magnetic flux and the magnetic field can be described as

$$\boldsymbol{B} = \hat{\mu} \cdot \boldsymbol{H} \tag{3}$$

where

$$\hat{\mu} = \begin{bmatrix} \mu & j\kappa & 0 \\ -j\kappa & \mu & 0 \\ 0 & 0 & 1 \end{bmatrix}.$$

In turn

$$\mu = 1 + \frac{4\pi\gamma^2 M H_i}{(\gamma H_i)^2 - \omega^2}$$

and

$$\kappa = \frac{4\pi\omega\gamma M}{(\gamma H_i)^2 - \omega^2}.$$

Also, one can write

$$\nabla \times \boldsymbol{H} = 0 \quad \text{and} \quad \nabla \times \boldsymbol{H}_0 = 0. \tag{4}$$

From the magnetostatic approximation of the previous equation, and using (1) and (2), some proper mathematical manipulations result in the following expression [7]

$$\int \nabla \cdot [j\omega\phi_0^* \boldsymbol{B} + \phi(j\omega \boldsymbol{B}_0)^*]\, dx = 0. \tag{5}$$

In this equation, ϕ and ϕ_0 are the magnetic potentials as obtained from (4) and are assumed to be independent of the z direction.

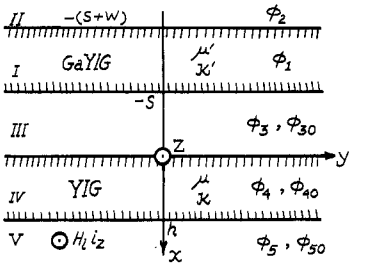

Fig. 1. Geometry of the problem.

The geometry of the problem considered can be seen from Fig. 1. It consists of two thin slabs. Slab IV has thickness h and the slab I has thickness w with a finite gap s in between them. The biasing magnetic field is assumed to be applied in the $+z$ direction, and thus the resulting magnetostatic surface wave is considered to be propagating in the $\pm y$ direction. The underlying idea of the present formulation can be stated as: the field quantities are assumed to be unperturbed in the presence of the large gap s in between the two slabs where, in fact, no coupling is considered; whereas, they become perturbed as the two slabs close each other. To proceed with the analysis, the following approximations are made: 1) The perturbation which occurs when the two slabs are near each other is assumed to affect only one surface of slab IV, i.e., the surface $x = 0$ and not the opposite surface $x = h$, and 2) the Poynting power flowing in the y direction is assumed to be considered only within slab IV. Thus the power flowing in open regions III and V are neglected. In the present analysis, these approximations can be supported in view of the physical nature of the surface waves.

Based on the aforementioned assumptions, the field distribution in the $-y$ direction of propagation is assumed to be $\exp[j(k^- y + \omega t)]$, where k^- denotes the propagation constant in the $-y$ direction, because the waves concentrate the energy on the $x = 0$ surface for propagating in the $-y$ direction of the present configuration [3]. Use of this distribution function in (5) results in

$$\Delta k^- = \frac{-j[\boldsymbol{B}(j\omega\phi_0^*) + \phi(j\omega \boldsymbol{B}_0)^*] \cdot \boldsymbol{i}_x \Big|_{x=0}}{4P_n} \tag{6}$$

where

$$\Delta k^- = k^- - k_0^{-*}$$

and

$$4P_n = \int_0^h [\boldsymbol{B}(j\omega\phi_0^*) + \phi(j\omega \boldsymbol{B}_0)^*] \boldsymbol{i}_y\, dx$$

$\boldsymbol{i}_x$ and $\boldsymbol{i}_y$ being the unit vectors in the $+x$ and $-y$ directions, respectively, and P_n is the power flow through slab IV. Equation (6) represents the surface perturbation formula for the magnetostatic-wave case. This expression is similar to the expression for the elastic surface-wave case in piezoelectric materials as developed by Auld [7].

Now referring to Fig. 1, the magnetic potentials in each separate region are defined as ϕ_1, ϕ_2, ϕ_3, ϕ_4, and ϕ_5 in

the perturbed condition and they are ϕ_{30}, ϕ_{40}, and ϕ_{50} in the unperturbed case.

All these magnetic potentials satisfy Laplace's equation

$$\nabla^2\phi = 0. \tag{7}$$

The solutions of the potential functions are obtained as

$$\phi_1 = (A \exp(k^- x) + B \exp(-k^- x)) \exp(jk^- y) \exp(j\omega t) \tag{8}$$

$$\phi_2 = C \exp(k^- x) \exp(jk^- y) \tag{9}$$

$$\phi_3 = (D \exp(k^- x) + E \exp(-k^- x)) \exp(jk^- y) \tag{10}$$

and

$$\phi_{30} = N \exp(k^- x) \exp(jk^- y) \tag{11}$$

where A, B, C, D, E, and N are the constants and an approximation that $k_0^- \approx k^-$ is made. By seeking the normal components of the magnetic-flux densities for each region, one can obtain from equations (8)–(11)

$$B_{1x} = k^-[(-\mu' + \kappa')A \exp(k^- x) + (\mu' + \kappa')B \exp(-k^- x)] \exp(jk^- y) \tag{12}$$

$$B_{2x} = -k^- C \exp(k^- x) \exp(jk^- y) \tag{13}$$

$$B_{3x} = -k^-(D \exp(k^- x) - E \exp(-k^- x)) \cdot \exp(jk^- y) \tag{14}$$

and

$$B_{30x} = -k^- N \exp(k^- x) \exp(jk^- y). \tag{15}$$

Here, μ' and κ' are the susceptibility tensors for slab I. These quantities are similar as defined in (3), except that the magnetic characteristics are different.

From

$$\nabla \cdot \boldsymbol{B} = \nabla \cdot (\hat{\mu} \cdot \boldsymbol{H}) = 0 \tag{16}$$

and

$$\nabla \cdot \boldsymbol{B}_0 = \nabla \cdot (\hat{\mu} \cdot \boldsymbol{H}_0) = 0 \tag{17}$$

a new variable ψ is defined as

$$\nabla \cdot \hat{\mu}\nabla(\phi_4 - \phi_{40}) = \nabla \cdot \hat{\mu}\nabla\psi = 0 \tag{18}$$

where ψ represents the slight variation of the magnetic potential in slab IV due to the closing in of the slab I. The solution of equation (18) can easily be written in the form, assuming the previous approximation that $k_0^- \approx k^-$,

$$\psi = (F \exp(-k^- x) + G \exp(k^- x)) \exp(jk^- y) \tag{19}$$

where F and G are constants. Based on the assumptions mentioned before, the magnetic perturbation on the $x = h$ surface of slab IV is negligible. Thus ψ must vanish in the infinite $+x$ direction, which means the value of G reduces to zero. Otherwise, for ψ to vanish for $x = +h$, the condition obtained from (19) is $G = -F \exp(-2k^- h)$. However, from the numerical results, the value of G was seen to be very small and hence can be considered zero for all practical purposes.

Also, from (16)–(18), one can obtain

$$\boldsymbol{B}_4 - \boldsymbol{B}_{40} = -\mu\nabla\psi \tag{20}$$

and the equivalent magnetic impedance $z_H(0)$ is assumed as

$$z_H(0) = \frac{Z_H(0)}{|Z_{H0}(0)|} = -jk\left(\frac{\phi_4}{B_{4x}}\right)_{x=0}$$

where

$$Z_H(0) = \left(\frac{\phi_{30}}{j\omega B_{3x0}}\right)_{x=0}. \tag{21}$$

To carry out the present analysis, the boundary conditions, as applied to the problem, are

$$\phi_1 = \phi_2 \qquad B_{1x} = B_{2x} \quad \text{at} \quad x = -(s + w) \tag{22}$$

$$\phi_1 = \phi_3 \qquad B_{1x} = B_{3x} \quad \text{at} \quad x = -s \tag{23}$$

$$\left.\begin{aligned} \phi_{30} &= \phi_{40} \qquad B_{30x} = B_{40x} \\ \phi_3 &= \phi_4 \qquad B_{4x} = B_{3x} \end{aligned}\right\} \quad \text{at} \quad x = 0. \tag{24}$$

Then the quantities B_{4x} and ϕ_4 are expressed in terms of ϕ_{30} by using (19), (21), and (24), and ultimately put into (6) to yield

$$\frac{\Delta k^-}{k^-} = \frac{-\omega[1 + \mu + \kappa][1 + jz_H(0)]}{1 - (\mu + \kappa)jz_H(0)} \frac{|\phi_{30}|^2}{4P_n}. \tag{25}$$

Here, the value of Δk^- is defined as $\Delta k^- = k^- - k_0{}^{*-} = k^- - k_0^-$, because the propagation constant in the case of the unperturbed field is always real as is discussed in the following section. Now, from (25), it can easily be seen that Δk^- becomes zero if $z_H(0)$ has the value j. Thus, it can be physically interpreted that the quantity $z_H(0)$ corresponds to the equivalent impedance of the outer magnetic circuit. This impedance can easily be evaluated by the substitution of (10), (14), and (24) in (21), and is

$$z_H(0) = \frac{-[z_H(-s) + j \tanh(k^- s)]}{jz_H(-s) \tanh(k^- s) - 1} \tag{26}$$

where, $z_H(-s)$ is the value of z_H at $x = -s$ and can be estimated from boundary conditions (22) and (23) when substituted with equations (8)–(10) and (12)–(14). Thus one gets the following expression

$$z_H(-s) = j \frac{\omega_0{}'^2 - \omega^2 + (\omega_h{}^2 - \omega^2 + 4\pi\omega\gamma M') \tanh(wk^-)}{(\omega_M{}'^2 - \omega^2 - 4\pi\omega\gamma M') \tanh(wk^-) + \omega_0{}'^2 - \omega^2}. \tag{27}$$

Here

$$\omega_M{}' = \gamma(H_i + 4\pi M')$$

$$\omega_h = \gamma H_i$$

and

$$\omega_0{}'^2 = \gamma^2 H_i(H_i + 4\pi M').$$

Finally, by putting (26) and (27) into (25), the complete perturbation formula is obtained as

$$\frac{\Delta k^-}{k^-} = \frac{-\omega[\omega_h + \omega_M - 2\omega][1 + jz_H(0)]}{\omega_h - \omega - j[\omega_M - \omega]z_H(0)} \frac{|\phi_{30}|^2}{4P_n^-}. \tag{28}$$

In the previous expression

$$z_H(0) = \frac{j}{Q}\{[\omega_h^2 - \omega^2 + 4\pi\omega\gamma M' + (\omega_M'^2 - \omega^2 - 4\pi\omega\gamma M')\tanh(k^- s)] \cdot \tanh(wk^-) + (\omega_0'^2 - \omega^2)(1 + \tanh(k^- s))\}$$

$$Q = \{(\omega_h^2 - \omega^2 + 4\pi\omega\gamma M')\tanh(k^- s) + \omega_M'^2 - \omega^2 - 4\pi\omega\gamma M'\} \cdot \tanh(wk^-) + (\omega_0'^2 - \omega^2)(1 + \tanh(k^- s))$$

and

$$\omega_M = \gamma(H_i + 4\pi M).$$

B. Unperturbed Solution

In the unperturbed case, the dispersion relation is obtained by applying the boundary conditions relating to the magnetic potentials ϕ_{30}, ϕ_{40}, and ϕ_{50} and is given by

$$\exp(-2k^- h) = \frac{(1+\mu)^2 - \kappa^2}{(1-\mu)^2 - \kappa^2}. \tag{29}$$

This is similar to the expression as obtained by Damon and Eshbach [3]. Also $k^- \approx k_0^-$, as may be obtained from the root of (29), is always real if one considers the no-loss case. Then, by expressing the values of B_0 and ϕ_0 within slab IV in terms of ϕ_{30} and using (6), one can easily obtain the power flow in the $-y$ direction which is given as

$$\frac{|\phi_{30}|^2}{4P_n^-} = \frac{-1}{\omega\left[\frac{2\omega_s}{\omega_s + \omega} - k^- h\,\frac{8\pi\gamma M(\omega_s - \omega)}{\omega_0^2 - \omega^2}\right]} \tag{30}$$

where

$$\omega_s = \gamma(H_i + 2\pi M).$$

Lastly, by substituting (29) and (30) in (28), the perturbed propagation constant is easily calculated.

III. Discussion on the Perturbed Air Gap and Slab Modes

In this section, the frequency dependence of the propagation constant for a magnetostatic surface wave affected by the magnetic perturbation is numerically estimated by using the perturbation formula of (28).

The properties of the slabs chosen for doing the experiment are as follows: slab IV is a polished single-crystal YIG (0.56 × 0.45 × 0.056 in cm) oriented in the (110) plane and the slab I is a polished Ga–YIG (0.967 × 0.402 × 0.053 in cm) oriented in the (100) plane. The different material constants chosen are as follows: $\gamma = 1.76 \times 10^7$ (Oe·s)$^{-1}$; $4\pi M$ (for YIG) = 1730 Oe; $4\pi M'$ (for Ga–YIG) = 400 Oe; $w = 0.053$ cm; $h = 0.056$ cm; and $H_i = 520$ Oe. With these numerical values, the dispersion diagram is obtained from (28)–(30) and is shown in Fig. 2. From the figure it can be seen that the curve for $s = 0.14$ cm almost resembles the curve obtained from the unperturbed solution of (29). Further, there are two sets of curves. One set lies between f_0 (3.05 GHz) and f_s (3.87 GHz)

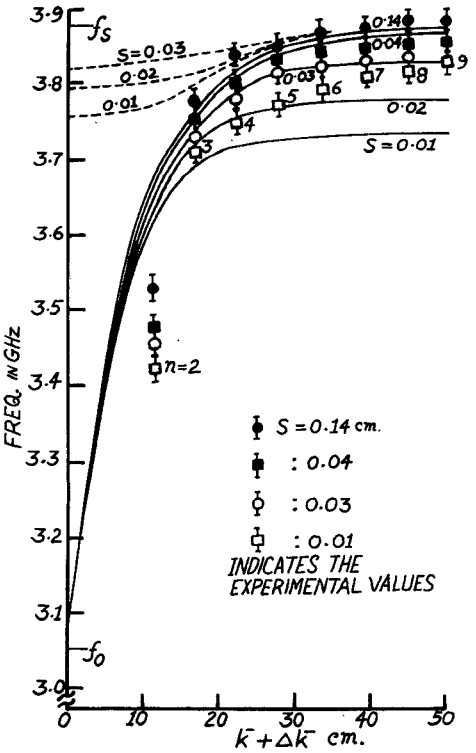

Fig. 2. Dispersion diagram and the related experimental results.

and has the characteristic that the curves droop down with the lowering of the s values. This mode can be designated as the "slab mode" due to the weak coupling of the magnetostatic surface waves propagating in the two slabs. The other set of curves lying in the frequency domain between 3.75 and 3.87 GHz corresponds mainly to the region $k^- + \Delta k^-$ less than 25 cm^{-1}. This mode is similar to the "air-gap mode" in a semi-infinite ferrite medium already discussed by one of the present authors [8]. The physical interpretation for the existence of the previous two types of modes, which are measured experimentally and discussed in Section IV, can be given as follows.

The layered structure of Fig. 1, though considered to be infinite in the $\pm y$ direction, has finite y dimension practically, and hence the surface waves propagating on the two slabs make traveling-wave-type resonances [9].

The generation of the two aforementioned types of modes can be clearly understood from the Fig. 3(a) and (b). With the applied magnetic field in the opposite direction $(-z)$ as compared to Fig. 1, the magnetostatic surface wave travels in a closed path around both the YIG and Ga–YIG slabs, i.e., between the $x = 0$, $x = h$ and the $x = -s$, $x = -(s + w)$ surfaces, respectively, to exhibit traveling-wave resonances. For the separation distance s in between the two slabs, about one wavelength long, the surface waves on the $x = 0$ and $x = -(s + w)$ surfaces couple weakly with each other and this phenomenon gives rise to the slab mode, which is sensitive to the magnetic perturbations. On the other hand, with the s value smaller than the thicknesses of the slabs concerned, the surface wave at $x = 0$ finds an easier way to return through the $x = -s$ surface and resonate. This produces the air-gap mode,

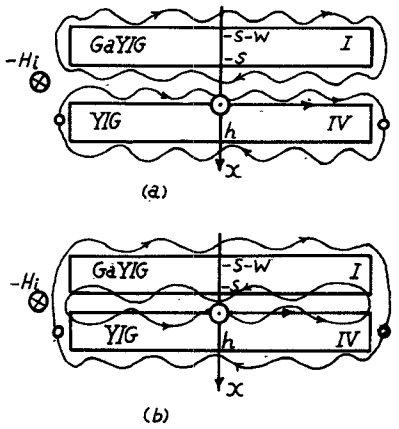

Fig. 3. The magnetostatic resonance of two types. (a) Weak coupling. (b) Tight coupling.

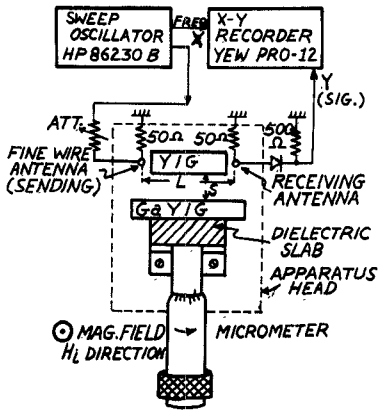

Fig. 4. The experimental setup.

though the slab mode may exist simultaneously due to the rather weak coupling between the surface waves traveling in the $x = h$ and $x = -(s + w)$ planes. But the present analysis is not fruitful enough for an explanation of the air-gap mode which is not sensitive to the perturbation.

IV. Experimental Results

The experimental setup can be clearly seen from Fig. 4. The power from the microwave sweep generator is supplied to the YIG slab through a fine-wire antenna attached to the side of it and is received by another similar antenna to send it to the X–Y recorder circuit. Both antenna circuits are grounded through a resistance of about 50 Ω. The Ga–YIG slab is held fixed on a micrometer which can adjust the air gap between the slabs, and the micrometer is assumed to be indifferent to the magnetic-field variations. Now the apparatus head is put under the influence of the electromagnets.

Thus the frequency characteristics of the magnetostatic surface wave can be recorded by the recorder with the frequency fed to the X terminal and the signal to the Y terminal. Here, the sweep frequency is chosen to be from 2.9 to 4.2 GHz and the magnetic-field intensity is adjusted to $H_0 = 620$ Oe.

Theoretically, the magnetostatic resonances that occur have to satisfy the relation [10]

$$k^- + \Delta k^- = \frac{n\pi}{\mathscr{L}}, \qquad n = 0,2,3,\cdots \tag{31}$$

where $\mathscr{L}$ is the length of the slab (= 0.56 cm, in the present case). This relation is good enough when one considers the resonance only at the $x = 0$ surface but not on the $x = h$ surface. However, in the present case, due to the weak coupling between the waves on the two slabs, the resonance conditions at the $x = 0$ and $x = h$ surfaces are assumed to be approximately equal. Of course, while doing the experiment, the frequency dependencies of the other measuring circuits, such as antennas, etc., are minimized. The experimental data thus obtained are plotted in Fig. 2. The resonance numbers depicted in the figure refer to the numbers defined in (31).

As can be seen from Fig. 2, the experimental points coincide with the theoretical ones for $n = 3,4,5$. However, there is a mismatch in the cases when $n = 2$ and for smaller s values ($s = 0.01$). The reasons for this can be explained as follows. First, the present analysis was carried out assuming a two-dimensional problem which does not give a good approximation, particularly at a low frequency like f_0 ($k^- + \Delta k^- \approx 0$), [3]. Secondly, with smaller s values, the perturbation approximation is thought to break down.

Next, to measure the frequency dependence of the resonances with fine variations in the s value, a rather narrow frequency band is chosen (from 3.72 to 3.98 GHz) and the s value is precisely adjusted below 0.01 cm by inserting into the air gap extremely thin mica plates. The results obtained are shown in the Fig. 5. It should be noted from the figure that for s values below 0.01 cm, the number of resonance peaks increases and the frequency intervals between each resonance grows narrower. The corresponding theoretical curves are also plotted by solving (28), where $k^- + \Delta k^-$ values satisfy the resonance condition of (31). In the figure, the solid line represents the slab mode and the dotted lines stand for the air-gap mode. The experimental curves are in approximate agreement with the theoretical curves for the resonance numbers 3,4,5,6. But, as can be seen, they are not in good agreement above $n = 7$. The reasons may be due to the effect of the demagnetizing field which arises when the two ferrite slabs of different magnetic saturations are brought into close proximity, and also to the anisotropy of the internal magnetic field, the theoretical estimation of which is rather complicated. The other reason may also be due to the Gaussian distribution of the RF magnetic field in the z direction, which has not been considered in the present analysis [11]. On the other hand, the resonances occurring between 3.8 and 3.86 GHz below $s = 0.01$ cm seems to be due to the air-gap mode [8]. Although these do not coincide exactly with the theoretical values, but from the tendency of these curves, the air-gap modes may be assumed to exist.

The measured difference between the magnetic field in the air and the inner magnetic field is $\bar{H}_0 = H_0 - H_i$, and is estimated to be (100 ± 10) Oe.

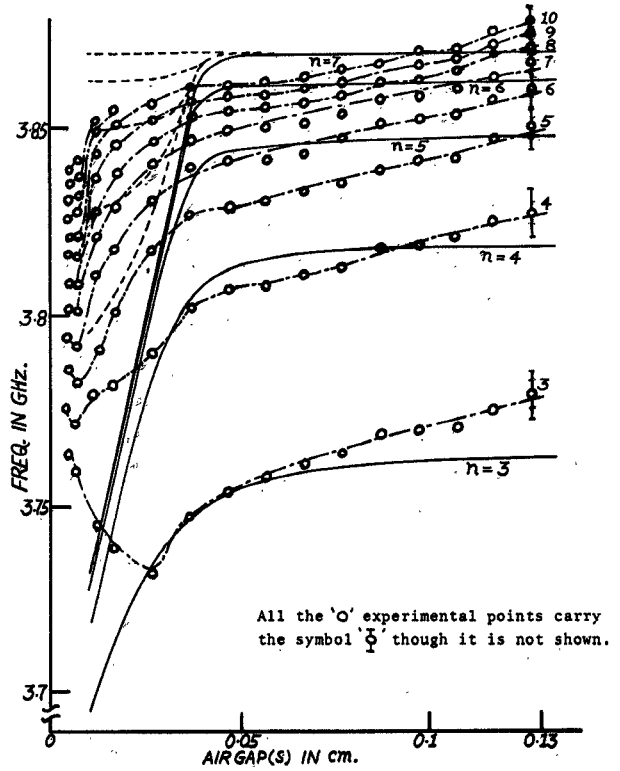

Fig. 5. Comparison between the theory and the experiment.

V. Theoretical Estimation of Group Delay

In this section, the group delay of the magnetostatic wave is considered theoretically to show how it is affected by the magnetic perturbation.

For simplicity, the quantity $jz_H(0)$ is nearly equal to -1, and $|\phi_{30}|^2/4P_n$ is assumed to be frequency independent. With this assumption, the group delay per unit length can be estimated from (28) as

$$\tau = \frac{\partial k^-}{\partial \omega} + \frac{\partial(\Delta k^-)}{\partial \omega} = \tau_0(1 + \Delta C), \quad \text{s/cm} \tag{32}$$

where

$$\tau_0 = \frac{\partial k^-}{\partial \omega}$$

and

$$\Delta C = \frac{1}{\tau_0}\frac{\partial(\Delta k^-)}{\partial \omega}.$$

Physically, τ_0 is the group delay in the unperturbed case and $\tau_0\,\Delta C$ is that in the perturbed case. Thus the expressions for τ_0 and ΔC can be obtained by the use of (28) and (29) as

$$\tau_0 = \frac{\omega}{h(\omega_s^2 - \omega^2)} \tag{33}$$

and

$$\Delta C = -\frac{|\phi_{30}|^2}{4P_n}\left\{\omega(1 + jz_H(0)) + \frac{k^-}{\tau_0} \cdot \left[1 + jz_H(0) + \omega\frac{\partial(1 + jz_H(0))}{\partial \omega}\right]\right\}. \tag{34}$$

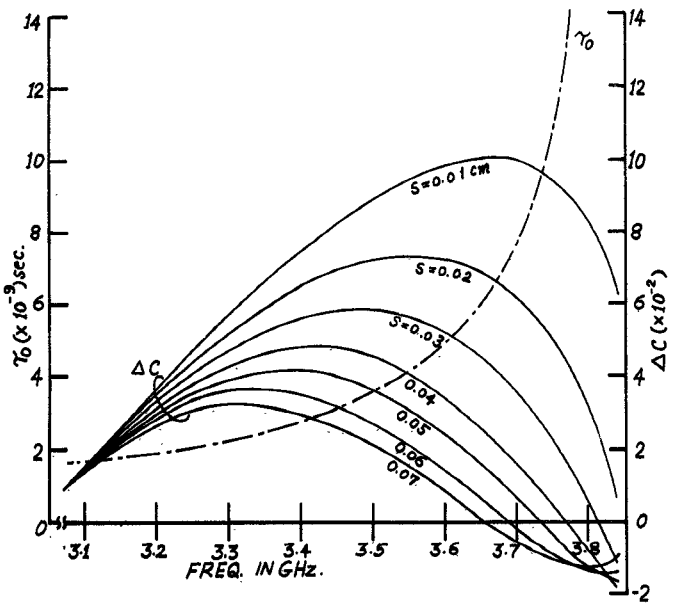

Fig. 6. Group delay as a function of frequency.

From the previous expressions, it is obvious that τ_0 is in inverse ratio to the slab thickness and becomes infinity as ω approaches ω_s. Also ΔC depends directly on the factors $1 + jz_H(0)$ and $|\phi_{30}|^2/4P_n$. To seek the value of τ_0 numerically, (33) is used with a magnetic field of 520 Oe and is plotted in Fig. 6 with the center line. As can be seen, a large delay appears as the frequency approaches 3.8 GHz. Also the value for ΔC is plotted with different values for s which are shown by solid lines in the figure. It should be noted that in the ordinate ΔC is plotted instead of $\tau_0\,\Delta C$ in order to demonstrate the effect of the perturbation. When the two slabs of different magnetic saturations are generally brought closer, the curves for ΔC show a tendency to have maximum value in the frequency interval 3.3 and 3.8 GHz. Thus the dispersive characteristics are weakened slightly in this region.

VI. Conclusion

The propagation characteristics of the magnetostatic waves associated with two ferrite slabs having different magnetic saturations are discussed using the perturbation method and the existence of two modes; that is, the slab mode and the air-gap mode have been shown. Some experiments have been performed using single-crystal YIG and Ga–YIG slabs and the experimental results are found satisfactory within the range of approximation of the perturbation theory. Further, from the theoretical estimation of the frequency dependence of the group delay, it has been found that the dispersive characteristics of group delay are weakly affected by the magnetic perturbation.

Thus it is concluded that the perturbation method is still unique in understanding the fundamental behavior of the magnetostatic surface waves and is promising enough for application to delay lines and the other complex signal-processing systems. The authors can foresee its further usefulness in more complex problems, such as in the

analysis of the gain of magnetostatic amplifiers employing a composite layered structure of semiconductors and ferrites [12].

ACKNOWLEDGMENT

The authors wish to thank T. Higuchi, a student of this University, for his help in setting up the experimental apparatus.

REFERENCES

[1] J. C. Sethares and M. R. Stiglitz, "Propagation loss and MSSW delay lines," *IEEE Trans. Magn.*, vol. MAG-10, pp. 787–790, Sept. 1974.
[2] J. D. Adam, J. M. Owens, and J. H. Collins, "Magnetostatic delay lines for group delay equalisation in millimetric waveguide communication systems," *IEEE Trans. Magn.*, vol. MAG-10, pp. 783–786, Sept. 1974.
[3] R. W. Damon and J. R. Eshbach, "Magnetostatic modes of a ferromagnetic slab," *J. Phys. Chem. Solids*, vol. 19, pp. 308–320, 1961.
[4] A. K. Ganguly, C. Vittoria, and D. Webb, "Interaction of surface magnetic waves in anisotropic magnetic slabs," *AIP Conference Proc., 20th Annual Conference on Magnetism and Magnetic Materials*, pp. 495–496, 1974.
[5] A. K. Ganguly and C. Vittoria, "Magnetostatic wave propagation in double layers of magnetically anisotropic slab," *J. of Appl. Phys.*, vol. 45, pp. 4665–4667, Oct. 1974.
[6] W. L. Bongianni, "*X* band signal processing using magnetic waves," *Microwave J.*, pp. 49–52, Jan. 1974.
[7] B. A. Auld, "Acoustic fields and waves in solids," vol. II, p. 271, Wiley-Interscience, 1973.
[8] M. Tsutsumi, "Magnetostatic surface wave propagation through the air gap between adjacent magnetic substrates," *Proc. IEEE*, vol. 62, pp. 541–542, April 1974.
[9] L. K. Brundle and N. J. Freedman, "Magnetostatic surface waves on YIG slab," *Elect. Letts.*, vol. 4, pp. 132–134, April 1968.
[10] M. Sparks, "Magnetostatic surface modes of a YIG slab," *Elect. Letts.*, vol. 5, pp. 618–619, Nov. 1969.
[11] M. Beni, L. Millanta, and N. Rubino, "Dispersion characteristics of the Gaussian surface-magnetostatic wave modes in ferrite slab," *Elect. Letts.*, vol. 11, pp. 374–375, Aug. 1975.
[12] N. S. Chang, S. Yamada, and Y. Matsuo, "Characteristics of MSSW propagation in a layered structure consisting of metals, dielectrics, a semiconductor and YIG," *Elect. Letts.*, vol. 11, pp. 83–84, Feb. 1975.

Different Representations of Dyadic Green's Functions for a Rectangular Cavity

CHEN-TO TAI, FELLOW, IEEE, AND PAWEL ROZENFELD, MEMBER, IEEE

Abstract—**Several different but equivalent expressions of the dyadic Green's functions for a rectangular cavity have been derived. The mathematical relations between the dyadic Green's function of the vector potential type and that of the electric type are shown in detail. This work supplements the one by Morse and Feshbach [1].**

I. INTRODUCTION

THE dyadic Green's function for a rectangular cavity has previously been studied by Morse and Feshbach [1]. The function which they introduced is of the vector potential type, hereby denoted by $\bar{G}_A$, corresponding to the dyadic version of the vector Green's function for the vector Helmholtz equation. Two forms of $\bar{G}_A$ were obtained by these authors. While one form is complete, the other one is not. These authors mentioned that the two forms are equivalent when a longitudinal part is added to the incompleted form, but the exact relations were not discussed.

In a recent paper, Rahmat-Samii [7] presented the dyadic Green's function of the electric type for rectangular waveguides and cavities, and introduced an auxiliary dyadic $\bar{g}_m$. This dyadic, however, is the dyadic Green's function of the vector potential type $\bar{G}_A$, as can easily be seen by comparing (1) in the present work with [7, eq. (9)]. As a result, [7, eq. (26)] for $\bar{g}_m$ is the same as our expression (10). The representation of the dyadic Green's functions for rectangular waveguides which is given in Rahmat-Samii's paper has previously been presented in [3] and for rectangular cavities in [6].

In this paper, we give a detailed derivation of several alternative representations of the dyadic Green's functions of both the vector potential type and the electric type for a rectangular cavity. Although the two types of functions are intimately related, it is more direct to use the function of the electric type that would bypass the tedious differentiation of discontinuous series for the evaluation of the fields in a source region.

II. DYADIC GREEN'S FUNCTIONS OF THE VECTOR POTENTIAL TYPE AND OF THE ELECTRIC TYPE

The classification of dyadic Green's functions of various types and kinds has previously been discussed [2], [3]. For the present work, it is sufficient to review two types of functions pertaining, respectively, to the vector potential function and the electric field. The dyadic Green's function

Manuscript received September 23, 1975; revised February 24, 1976. The work of one of the authors (C.T.T.) was supported by the Harry Diamond Laboratories, while the work of the other author (P.R.) was supported by the Institute of Space Research (INPE), Brazil.

C. T. Tai is with the Radiation Laboratory, Department of Electrical and Computer Engineering, University of Michigan, Ann Arbor, MI 48104.
P. Rozenfeld is with the Institute of Space Research (INPE), São José dos Campos, SP, Brazil.